AIAA JOURNAL
Vol. 47, No. 10, October 2009

Criteria for Vortex Breakdown Above High-Sweep Delta Wings

Michael Jones,* Atsushi Hashimoto,† and Yoshiaki Nakamura‡
Nagoya University, Nagoya 464-8603, Japan

DOI: 10.2514/1.37177

The intention of the present work is to relate the theory for vortex breakdown, derived for breakdown observed in simple geometries, to the breakdown over a highly swept delta wing. Specifically, the appearance of negative azimuthal vorticity and the origin of this vorticity are considered. In addition, the helix angle criterion, associated with a change in criticality of the vortex core, is related to the onset of breakdown. Two delta wings are considered: a static delta wing with sweep angle of 76 degrees and a pitching delta wing with sweep angle of 70 degrees; both cases are modeled computationally. In the static case, the existence of breakdown is associated with the presence of an upstream change in sign of the azimuthal vorticity, consistent with analyses for simpler geometries. This negative azimuthal vorticity is shown to arise by a similar mechanism to that proposed for breakdown in a pipe. A transition in criticality of the delta wing vortex is also shown to be linked with the appearance of breakdown.

Nomenclature

Cp	=	pressure coefficient
c	=	delta wing root-chord length
f	=	pitching frequency
k	=	pitching reduced frequency ($2\pi fc/u_\infty$)
p	=	pressure
Re	=	Reynolds number ($u_\infty c/\nu$)
r	=	radial coordinate
r_c	=	vortex core radius
u_k	=	velocity ($k = x, r, \phi$)
u_∞	=	freestream velocity
x	=	axial coordinate
$\dot{\alpha}$	=	pitching rate
β	=	pseudocompressibility parameter
Γ_0	=	freestream circulation
ν	=	kinematic viscosity
ρ_0	=	density
ϕ	=	azimuthal coordinate
Ω	=	swirl ratio ($\Gamma_0/r_c u_\infty$)
ω_k	=	vorticity ($k = x, r, \phi$)

I. Introduction

THE first report of vortex breakdown of which the authors are aware is an observation by Wilcke, quoted by Maxworthy [1]. In that study, breakdown was observed in a simply constructed version of the torsionally driven cylinder (TDC). The phenomenon was sufficiently interesting to be mentioned in Wilcke's publication; breakdown acquired more practical importance when it was reported to occur above swept delta wings in the often-quoted study by Peckham and Atkinson [2]. Breakdown for a delta wing has been shown to result in a dramatic loss of lift, transient pitching and rolling moments, and for real aircraft, a turbulent flow downstream which has consequences for airframe components. However, since the report by Peckham and Atkinson, most theory for breakdown has been derived from simple geometries, such as the torsionally driven cylinder and pipe. (Reviews of the progress made in the understanding of breakdown include Leibovich [3], Delery [4], Althaus et al. [5], and Escudier [6].) For simple geometries, the phenomenon appears to be associated with a transition in the waveguide nature of a vortical flow. This transition results in the local trapping and amplification of disturbances at a particular location in the vortex core, where the upstream supercritical flow transitions to a subcritical flow (see, for example, Darmofal and Murman [7], Randall and Leibovich [8], and Rusak et al. [9]).

However, there is still disagreement regarding the relationship between the phenomenon observed at low Reynolds numbers in confined geometries (especially the torsionally driven cylinder) and that which manifests over delta wings at more realistic Reynolds numbers. Some researchers have questioned whether the phenomenon observed in the torsionally driven cylinder should be placed in the same class as the phenomenon produced over delta wings [3,10]. In particular, the torsionally driven cylinder generally produces an axisymmetric nonhysteretic form of breakdown, whereas for delta wings, breakdown has been shown to be primarily three-dimensional and displays significant hysteresis with regard to breakdown location.[§] More akin to breakdown over delta wings is the breakdown manifest in open pipes. For open pipes, breakdown also displays hysteresis at sufficiently high Reynolds number [12,13], but at low Reynolds number, the hysteresis disappears and breakdown evolves similarly to the case for the torsionally driven cylinder [14]. Hence, Reynolds number is critical to not only the onset of breakdown but also to the characteristics of the breakdown that appears.

Despite the considerable progress made in development of the fundamental theory for breakdown, this understanding has not yet resulted in control measures. Current control measures rely on manipulation of either the vortex swirl ratio or the pressure gradient above the wing [15]. Although effective to varying degrees, these control measures do not rely on an understanding of the mechanism for breakdown and hence do not take advantage of the considerable amount of work invested in deriving the theory.

Rusak and Lamb [16] showed that the swirl ratio (the ratio of the maximum azimuthal velocity to the maximum axial velocity in the vortex), previously used to indicate the susceptibility of a flow to breakdown in open pipes, could be used to predict the onset and location of breakdown over slender delta wings. The intention of the current work is to further consider how current explanations for vortex breakdown in simple geometries, in terms of azimuthal vorticity dynamics and the helix angle criterion, may be related to the more practically relevant phenomena produced above a delta wing.

Received 17 February 2008; revision received 28 April 2009; accepted for publication 30 April 2009.

*Visiting Researcher, Department of Aerospace Engineering. Member AIAA.

†Graduate Student, Department of Aerospace Engineering. Member AIAA.

‡Professor, Department of Aerospace Engineering. Member AIAA.

§The question of the absence of hysteresis for the torsionally driven cylinder flow has been addressed in a previous work by one of the authors [11]; it appears to be a result of the low Reynolds numbers at which TDC experiments are conducted. The collapse of the hysteresis loop has also been observed for pipes at an equivalent Reynolds number.

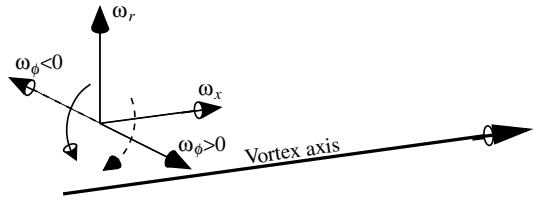

Fig. 1 Vorticity orientation definitions.

II. Azimuthal Vorticity Dynamics and the Criticality Criterion

Lopez [17] and Brown and Lopez [18] showed that a change in sign of the negative azimuthal vorticity upstream is a necessary condition for the onset of axisymmetric vortex breakdown. (Rusak [19] showed that this is equivalent to the condition that the derivative of the total head with the stream function must be positive.) For clarity, the sense of the azimuthal vorticity ω_ϕ is drawn in Fig. 1. The axial, radial, and azimuthal components are drawn in their standard orientations. Solid and dashed curves represent the positive and negative senses of vorticity, respectively. For a vortical structure in which the axial velocity is aligned with the vortex axis, from Fig. 1 it can be seen that the sense of the velocity associated with *negative* azimuthal vorticity (the dashed arrow) tends to oppose the axial flow. Hence, negative azimuthal vorticity may be associated with a slowing of the axial flow and, with sufficient intensity, the eventual onset of stagnation and recirculation.

In addition, for swirling flow in a finite pipe at high Reynolds numbers, it has been shown that the onset of breakdown is consistent with the development of instability in the flow at a critical level of swirl [20,21]. When the swirl of the flow is sufficient that infinitesimal disturbances can travel upstream, these disturbances become trapped at the critical location and amplify. Darmofal [22,23] described how this disturbance-trapping phenomenon can result in amplification of negative azimuthal vorticity in a vortical structure and lead eventually to breakdown. The analysis is based on Eq. (1), which describes the generation of azimuthal vorticity:

$$\frac{\mathrm{D}\omega_\phi}{\mathrm{D}t} = \omega_r \frac{\partial u_\phi}{\partial r} + \omega_x \frac{\partial u_\phi}{\partial x} - \frac{u_\phi \omega_r}{r} + \frac{u_r \omega_\phi}{r} \tag{1}$$

The four terms on the right-hand side correspond to two mechanisms. The first three terms describe the local generation of azimuthal vorticity by vortex filament turning (or tilting), and the fourth term describes the amplification of azimuthal vorticity by stretching. A geometrical description of these mechanisms is provided in Fig. 2.

Equation (1) hence provides a mechanism for the generation of negative ω_ϕ, and this mechanism was described by Darmofal [22]. The initial appearance and subsequent amplification (via feedback) of negative azimuthal vorticity was shown to be associated with the appearance of a recirculation region on the vortex core: the axisymmetric form of breakdown. Because the analysis has previously only been applied to simple axisymmetric flows, the first intention of the current analysis is to determine how well this description applies to the flow produced above a delta wing at incidence.

In addition to the vorticity dynamics, we also consider the delta wing vortex criticality. Previous work [4,24] has shown that the onset of breakdown can be linked to a change in the criticality of the vortical flow, and this change can be determined from the maximum helix angle γ (in the present work, γ is simply defined as the arctangent of the azimuthal velocity u_ϕ divided by the axial velocity u_x). Benjamin [24] showed that for a Rankine vortex, the transition in criticality occurs at a swirl ratio of $\Omega = 1.20$, which corresponds to a maximum helix angle of 50 deg. Spall et al. [25] conducted a summary of previous measurements of the Rossby number (equivalent to an inverse swirl) of breakdown-susceptible flows. For leading-edge-type vortices, breakdown appeared in experiments at a Rossby number equivalent to a helix angle of approximately 45 deg. Hence, for the current case, the critical helix angle may be closer to $\gamma = 45$ deg.

III. Computational Method and Problem Setup

For both the steady and pitching delta wing cases, implementations of the pseudocompressibility method were used to calculate the flowfield. However, the actual codes and the wing geometries used for each case were different.

Background to the pseudocompressibility method used is given by Kwak et al. [26], for example. The principle is described subsequently. The continuity and momentum equations for incompressible flow are expressed in Eqs. (2) and (3), respectively:

$$\frac{\partial u_i}{\partial x_i} = 0 \tag{2}$$

$$\frac{\partial u_k}{\partial t} + \frac{\partial u_k u_i}{\partial x_i} = -\frac{1}{\rho_0}\frac{\partial p}{\partial x_k} + \nu \nabla^2 u_k \tag{3}$$

where x_k are the Cartesian coordinates ($k = 1, 2, 3$), u_k are the respective velocities, p is the pressure, ρ_0 is the density, and ν is the kinematic viscosity. An artificial compressibility term is introduced into the equations to transform this elliptic system into the hyperbolic system of Eqs. (4) and (5):

$$\frac{\partial p}{\partial \tau} + \frac{\partial \beta u_i}{\partial x_i} = 0 \tag{4}$$

$$\frac{\partial u_k}{\partial \tau} + \frac{\partial u_k}{\partial t} + \frac{\partial u_k u_i}{\partial x_i} = -\frac{1}{\rho_0}\frac{\partial p}{\partial x_k} + \nu \nabla^2 u_k \tag{5}$$

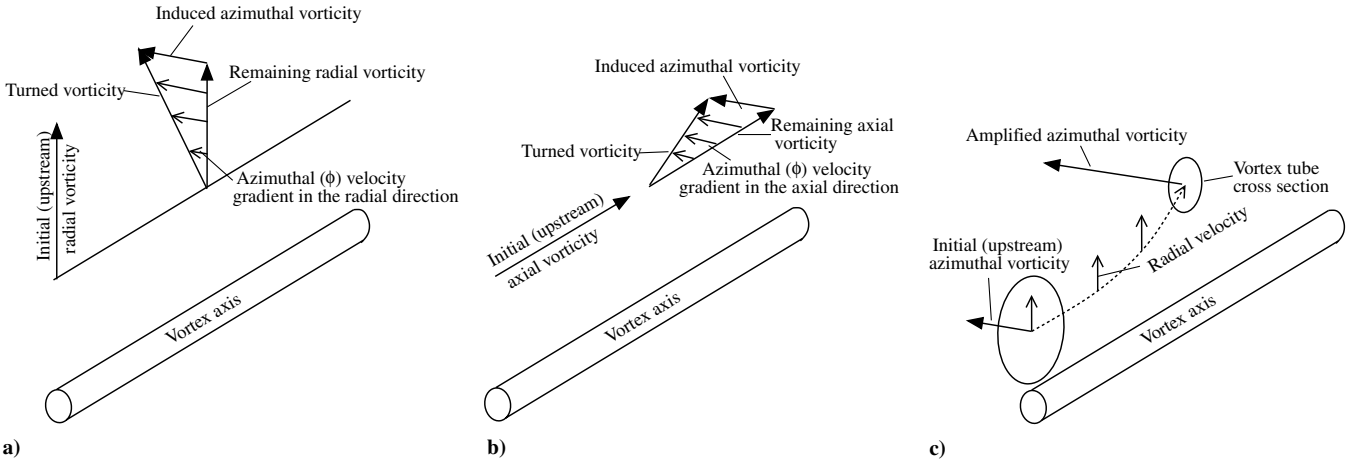

Fig. 2 Generation of ω_ϕ by manipulation of existing vorticity: a) turning of radial vorticity into the azimuthal direction, b) turning of axial vorticity into the azimuthal direction, and c) stretching of existing azimuthal vorticity.

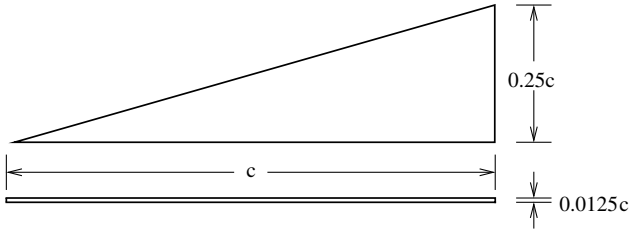

Fig. 3 Delta wing geometry.

where β is a constant and controls the speed of the pressure wave in this pseudocompressible model. A steady solution (in τ) is obtained for each real time step t. The result is a faster pressure-field calculation; the speed of convergence and stability are controlled by the choice of β.

A finite volume formulation was implemented, and time-marching of the Navier–Stokes equations was performed using the lower–upper symmetric Gauss–Seidel method. For determination of the inviscid flux, flux vector splitting with MUSCL interpolation and Barth–Jesperson curve limiting was used, with second-order central differencing for the viscous flux. For the pitching delta wing case, the inviscid flux was determined using Roe's approximate Riemann solver with third-order MUSCL method with the van Albada limiter. A second-order backward-difference expression was added to achieve second-order accuracy in time.

The wing geometry used for the steady-case computations is shown in Fig. 3. The delta wing has a sweep angle of 76 deg and a thickness of $0.0125c$, where c is the wing root-chord length, and has a rectangular leading edge. The wing is symmetric about the root chord, and only one-half of the wing was modeled, with a symmetry plane at the root chord. A Reynolds number of $Re = 2.7 \times 10^5$ was used.

IV. Validation

Computations for angles of attack (AOA) of 10 to 40 deg are presented. Experimental data were obtained in a parallel study using a wind tunnel at Nagoya University for a delta wing with identical planform. The sting used to support the wing was installed at the rear of the delta wing to minimize its effect on the flow; the sting was not modeled in the computational study.

In the experiment, surface pressure measurements were obtained for both the pressure and suction surfaces. The computational pressure coefficient Cp values are compared with those derived from the experiment in Fig. 4.

For AOA > 20 deg, the flow was observed to contain vortex breakdown; the flow downstream of breakdown becomes time-dependent; hence, for AOA > 20 deg, the computational data are averaged in time. The overall agreement between the computations and experiment is good; however, for AOA > 10 deg at the $0.4c$ chord station, the computed Cp is consistently high. The reason for this discrepancy is unclear. However, because the breakdown bubble is close to the $0.4c$ location for AOA $= 40$ deg, a small error in the location of breakdown could bring about a large error in Cp for that case. The drop in peak Cp for AOA $= 30$ deg at $x/c = 0.8$ and for AOA $= 40$ deg at $x/c = 0.6$ and 0.8 is well predicted; this drop is associated with the presence of breakdown upstream.

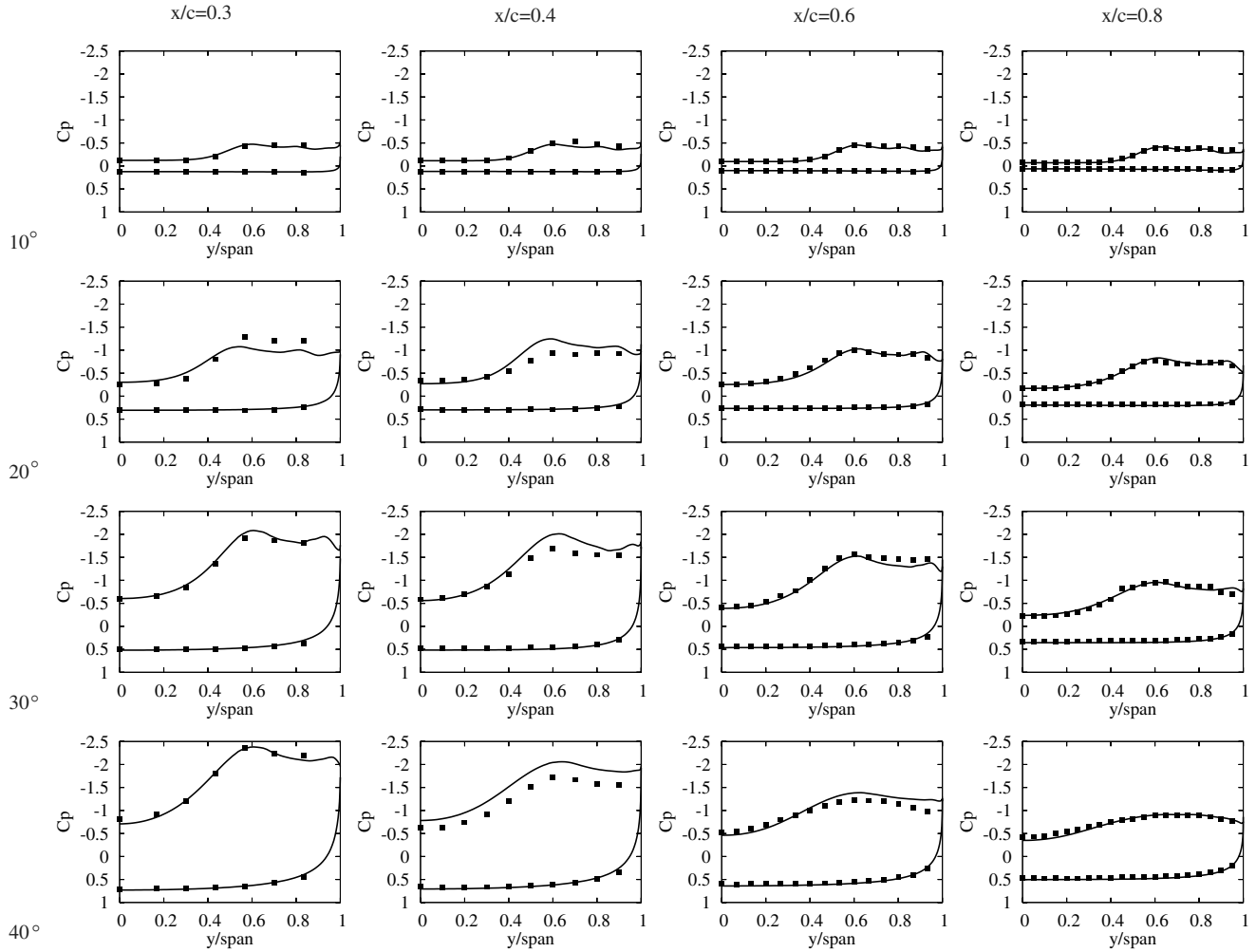

Fig. 4 Validation of the computational results using measurements of pressure coefficient. Points represent *Cp* calculated from pressure taps on the wing surface, and solid lines the equivalent computational results. Values are plotted in the spanwise *y* direction for AOA = 10 to 40 deg (top to bottom) and $x/c = 0.3$ to 0.8 (left to right), where *c* is the root-chord length.

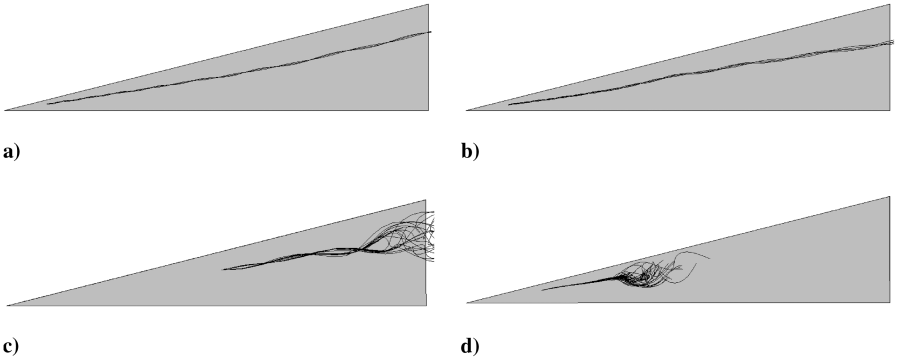

Fig. 5 Visualization of the vortex core above the delta wing: a) AOA = 10 deg, b) AOA = 20 deg, c) AOA = 30 deg, and d) AOA = 40 deg.

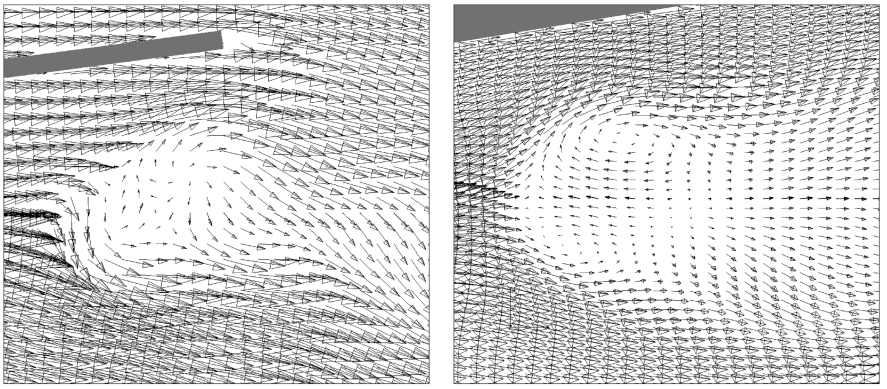

Fig. 6 Visualizations of breakdown: a) AOA = 30 deg and b) AOA = 40 deg.

V. Flow Visualization

For all angles of attack, the vortex cores generated in the computations are visualized in Fig. 5. For AOA = 10 and 20 deg, because the flow is steady, streamlines are plotted. For AOA = 30 and 40 deg, particle path lines are plotted. The presence of breakdown is apparent for AOA = 30 and 40 deg. In addition, cross sections in Fig. 6, which pass through the vortex core axis, reveal the flow in the breakdown region (the solid bars indicate the wing; the viewing direction is from the side). For AOA = 30 deg, only a spiral-type breakdown is observed; although there is some reversed flow, a bubble structure is not evident. At AOA = 40 deg, a structure more akin to an asymmetric bubble can be seen; there is a well-defined recirculation present in the interior of the bubble.

VI. Results: Vorticity Dynamics

In the following analysis, we are primarily interested in the flow in the vicinity of the vortex core. In Fig. 7, for AOA = 40 deg, the flow is visualized on planes perpendicular to the vortex axis in the region upstream of breakdown; the rightmost plane is located at the axial flow stagnation point. Contours of azimuthal velocity are plotted. The vortex core can be seen to be approximately axisymmetric close to its axis. Hence, for the following analysis, it is possible to assume axisymmetry to the point at which breakdown evolves (i.e., near the stagnation point).

Making use of this assumption, we conduct the analysis on a longitudinal cross section through the vortex, schematically represented in Fig. 8. The base of the plane is placed on the vortex axis, and the axis is approximately straight upstream of breakdown (see Fig. 5).

A. AOA = 30 Degrees

First, we consider the AOA = 30 deg case. Breakdown is present at this angle of attack (hence, the flowfield is unsteady), and so the velocity field is averaged in time over a full cycle of the spiral mode. In Fig. 9a, contours of axial velocity u_x are plotted, and in Fig. 9b, contours of azimuthal vorticity ω_ϕ are plotted. In these plots, and in all of the contour plots to follow, positive contours are represented by solid lines, and negative contours are represented by dashed lines. The direction of the flow is from left to right.

The plot of Fig. 9a reveals a rapidly decreasing axial velocity along the vortex axis from approximately $x = 0$, leading eventually to stagnation and flow reversal (i.e., breakdown) at approximately $x = 0.19$. This change in the nature of the vortex core is also evident in the plot of ω_ϕ, which is initially positive upstream of breakdown, but progressively reduces, and eventually becomes negative (near the axis) just upstream of the location at which breakdown occurs. This initial observation is consistent with the general theory described by Brown and Lopez [18] and Darmofal [22] and is also similar to the experimental observation of Özgören et al. [27] for a delta wing.

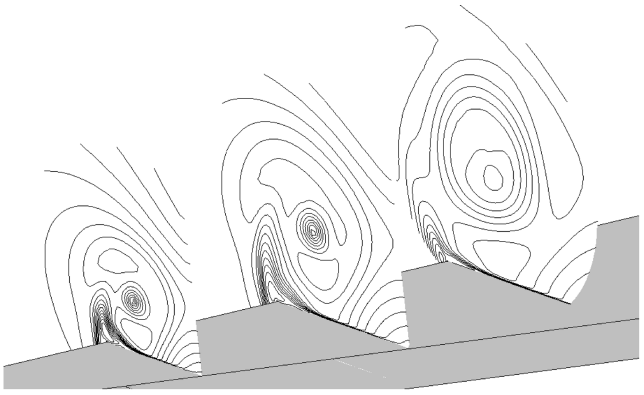

Fig. 7 Planes showing contours of azimuthal velocity u_ϕ for AOA = 40 deg; 16 contours at levels from $u_\phi = -0.88$ to $u_\phi = 1.67$ are shown.

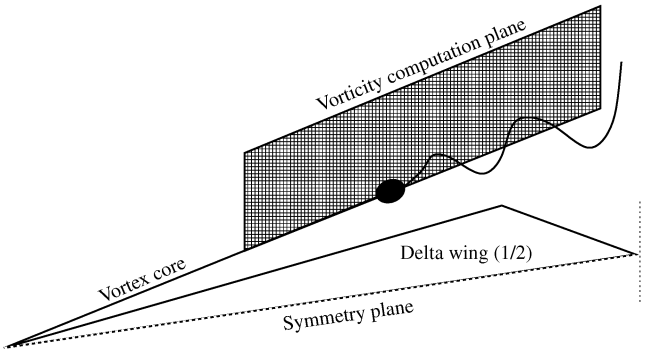

Fig. 8 Vorticity calculation plane.

We compare with observations for a pipe similar to that used in the analysis by Darmofal [23]. The inlet velocity profile is based on that observed experimentally for a q-vortex (see, for example, Leibovich [3]):

$$u_x(0) = 1 + \Delta u e^{-r^2} \qquad u_r(0) = 0 \qquad u_\phi(0) = \frac{\Omega}{r}[1 - e^{-r^2}] \quad (6)$$

where $u_x(0)$, $u_r(0)$, and $u_\phi(0)$ are the axial, radial, and azimuthal components of velocity, respectively, imposed at the inlet, as functions of the radial distance r. $\Delta u = 0$ for this case, the Reynolds number is $Re = 600$, and the swirl ratio $\Omega = 1.49$. The boundary at high r is a slip wall.

A result containing breakdown is shown in Fig. 10. A closed-bubble breakdown is evident in the streamline plot of Fig. 10a. As can be seen from the contours of ω_ϕ in Fig. 10b, for the pipe flow, there is also a change in sign of ω_ϕ just upstream of breakdown. In this axisymmetric pipe, a vortex core reforms downstream of breakdown, whereas above the delta wing, due to the onset of the spiral mode, any remaining vortex moves off the plane axis.

The origin of the negative azimuthal vorticity concentration can be determined by plotting the ω_ϕ production terms of Eq. (1). These terms for the delta wing are shown in Fig. 11 and are shown for the pipe in Fig. 12. For reference, the azimuthal vorticity contour plot is reproduced in both figures.

In Fig. 11c, the plot of total ω_ϕ generation reveals a local concentration of negative ω_ϕ production from $x = 0.1$. This local production results in the rapid reduction in azimuthal vorticity shown in Fig. 11b. The origin of this vorticity generation can be determined by consideration of the turning and stretching terms of Eq. (1), plotted in Figs. 11d and 11e.

For breakdown in the open pipe, the feedback mechanism has been shown to begin with the turning of vorticity into the azimuthal direction [23], and this is suggested in Fig. 11d, in which the total contribution from the turning terms is plotted (the contour level extrema are held constant for the plots of Figs. 11c–11e). This negative ω_ϕ then undergoes some stretching, which is apparent in Fig. 11e. However, the amplitude of the stretching is small relative to the contribution from turning.

In Figs. 12a–12d the equivalent quantities to those shown in Figs. 11b–11e are plotted for the pipe flow. Similarly to the observation for the delta wing, there is a concentration of negative ω_ϕ generation just upstream of breakdown (Fig. 12b). As for the delta wing, after the initial creation of azimuthal vorticity by turning (Fig. 12c), stretching results in additional azimuthal vorticity generation (Fig. 12d).

The breakdown process for both cases is hence initiated by turning. We can identify the type of vorticity being turned by splitting

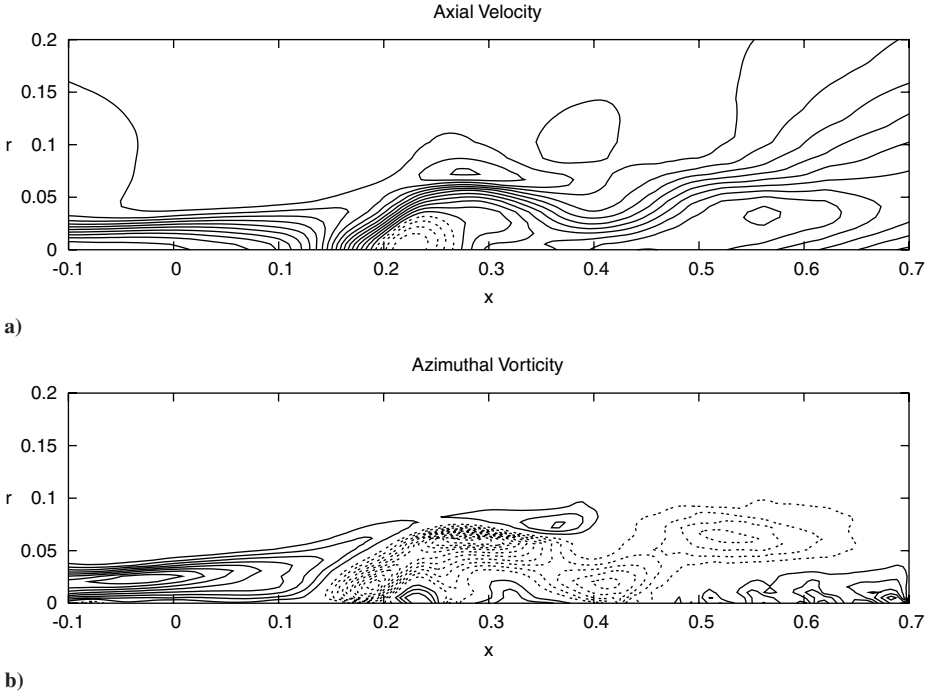

Fig. 9 Delta wing vortex for AOA = 30 deg: a) u_x and b) ω_ϕ.

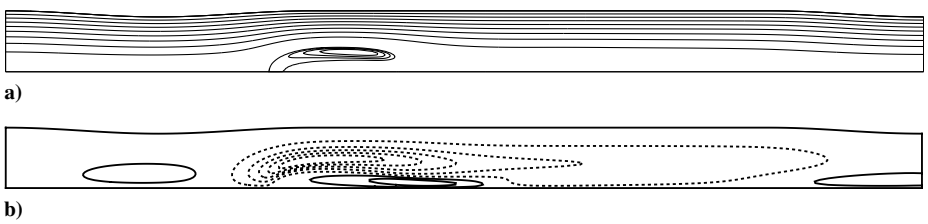

Fig. 10 Pipe a) streamlines and b) ω_ϕ.

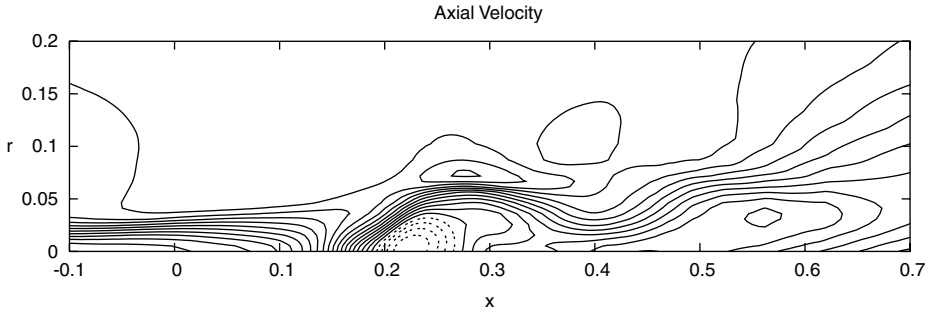

a)

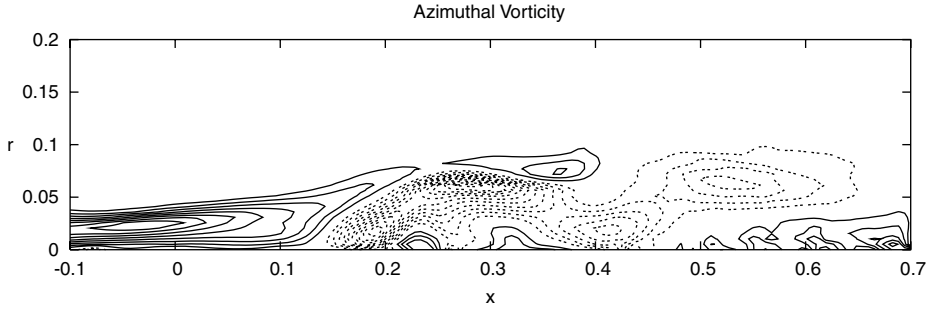

b)

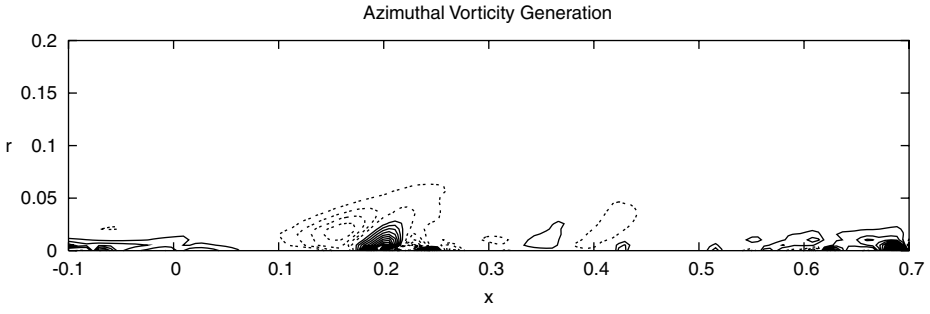

c)

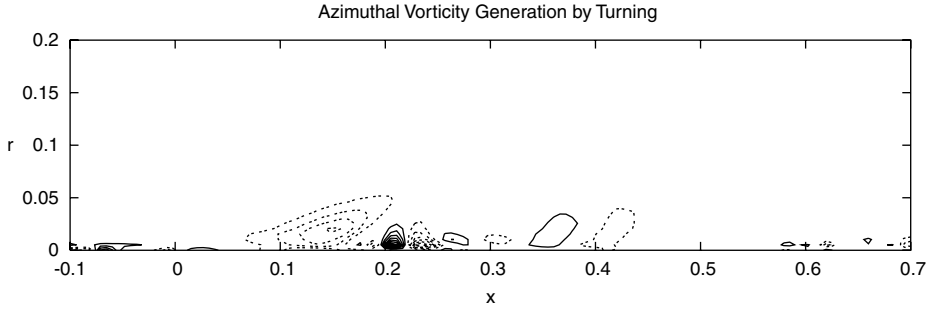

d)

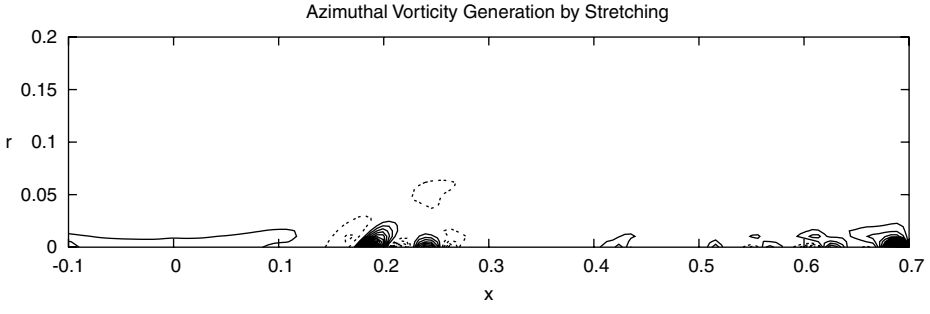

e)

Fig. 11 Delta wing vortex ω_ϕ generation for AOA $= 30$ deg: a) axial velocity, b) ω_ϕ, c) total ω_ϕ generation ($D\omega_\phi/Dt$), and d) ω_ϕ generation by turning ($\omega_r \partial u_\phi/\partial r + \omega_x \partial u_\phi/\partial x - u_\phi \omega_r/r$); e) ω_ϕ generation by stretching ($u_r \omega_\phi/r$).

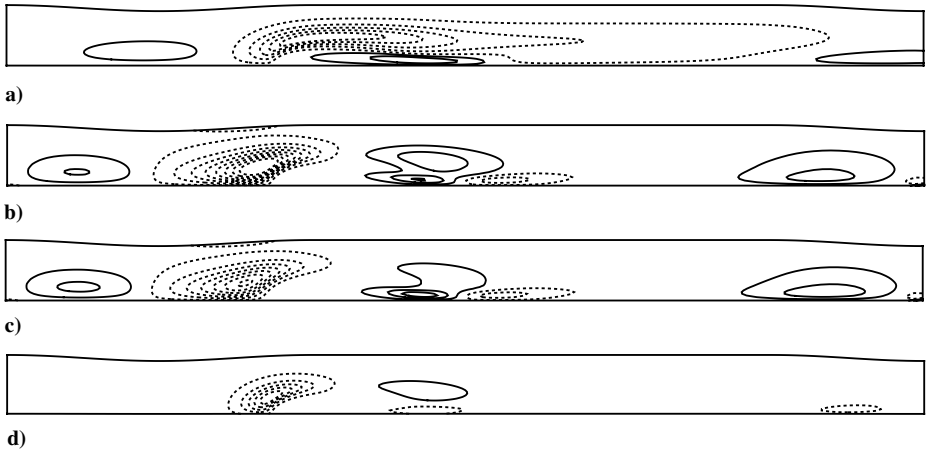

Fig. 12 Pipe ω_ϕ generation: a) ω_ϕ, b) total ω_ϕ generation ($D\omega_\phi/Dt$), c) ω_ϕ generation by turning ($\omega_r \partial u_\phi/\partial r + \omega_x \partial u_\phi/\partial x - u_\phi \omega_r/r$), and d) ω_ϕ generation by stretching ($u_r \omega_\phi/r$).

the turning term into its components: the contribution from turning of axial vorticity and that from turning of radial vorticity (see Fig. 13). Axial vorticity dominates in the vortex core; hence, at the beginning of the analysis, the axial vorticity is suspected to be the major contributor to negative ω_ϕ generation. In fact, it can be seen from Fig. 13a that turning of axial vorticity appears to be the only contributor to negative ω_ϕ production upstream of breakdown. The turning of radial vorticity leads to production of positive ω_ϕ and hence opposes the onset of breakdown.

B. AOA = 40 Degrees

For AOA = 30 deg, breakdown was manifest as a spiral mode with weak flow reversal and no axisymmetric bubble was observed. In contrast, for AOA = 40 deg, an axisymmetric bubble could be seen upstream of a spiral mode (see Fig. 6). Because it has been suggested that the bubble and spiral forms may be distinct phenomena (see, for example, Leibovich [3], Hall [28], and Goldshtik and Hussain [10]), in the following, we test whether the previous analysis also holds for the bubble form of breakdown.

Figure 14 shows contour plots of the axial velocity, negative ω_ϕ, and negative ω_ϕ production terms. As in the case of AOA = 30 deg, just upstream of breakdown (the negative contours in Fig. 14a), ω_ϕ becomes negative (Fig. 14b). The origin of this negative ω_ϕ is apparent in Fig. 14c, in which local production due to turning and stretching again results in local negative ω_ϕ generation just upstream of breakdown. From Fig. 14d, the dominant term in negative ω_ϕ production is again turning; the contribution from stretching (Fig. 14e) appears to be relatively minor.

The components of the turning term are represented in Fig. 15. As for the AOA = 30 deg case, only the turning of axial vorticity contributes to negative ω_ϕ production, and the turning of radial vorticity again opposes negative ω_ϕ production and hence opposes the onset of breakdown.

C. AOA = 10 Degrees

A solution without breakdown is provided for comparison with the higher-AOA flows. In Fig. 16, we plot the axial velocity and azimuthal vorticity for AOA = 10 deg.

In this case, no breakdown is present, and ω_ϕ remains positive throughout most of the vortex core. There is a small region of negative ω_ϕ near the axis, but it is too close to the axis to be distinguishable

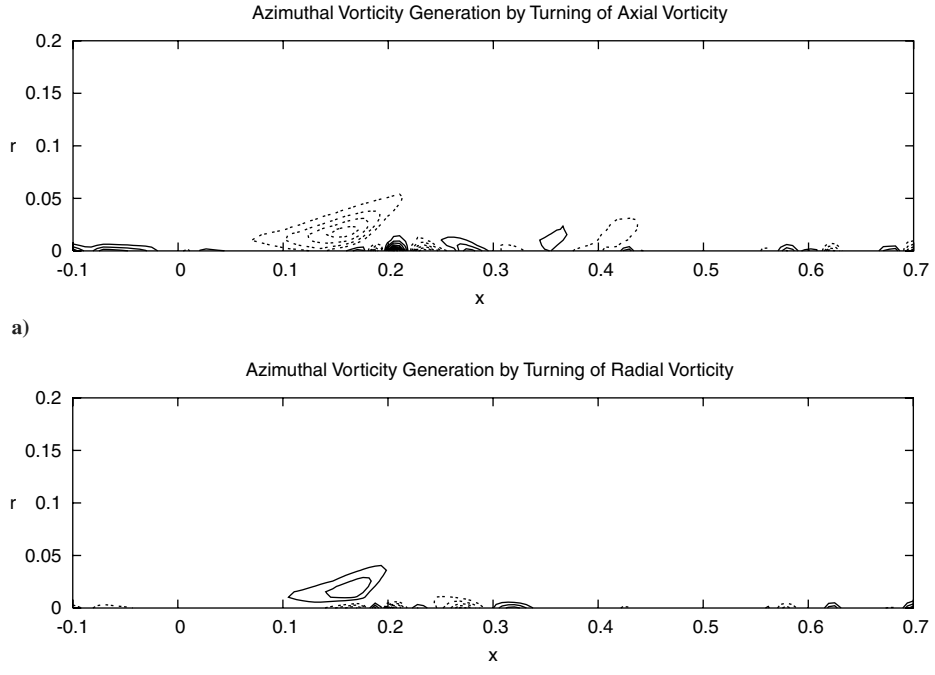

Fig. 13 Delta wing vortex ω_ϕ generation by turning for AOA = 30 deg: a) turning of axial vorticity ($\omega_x \partial u_\phi/\partial x$) and b) turning of radial vorticity ($\omega_r \partial u_\phi/\partial r - u_\phi \omega_r/r$).

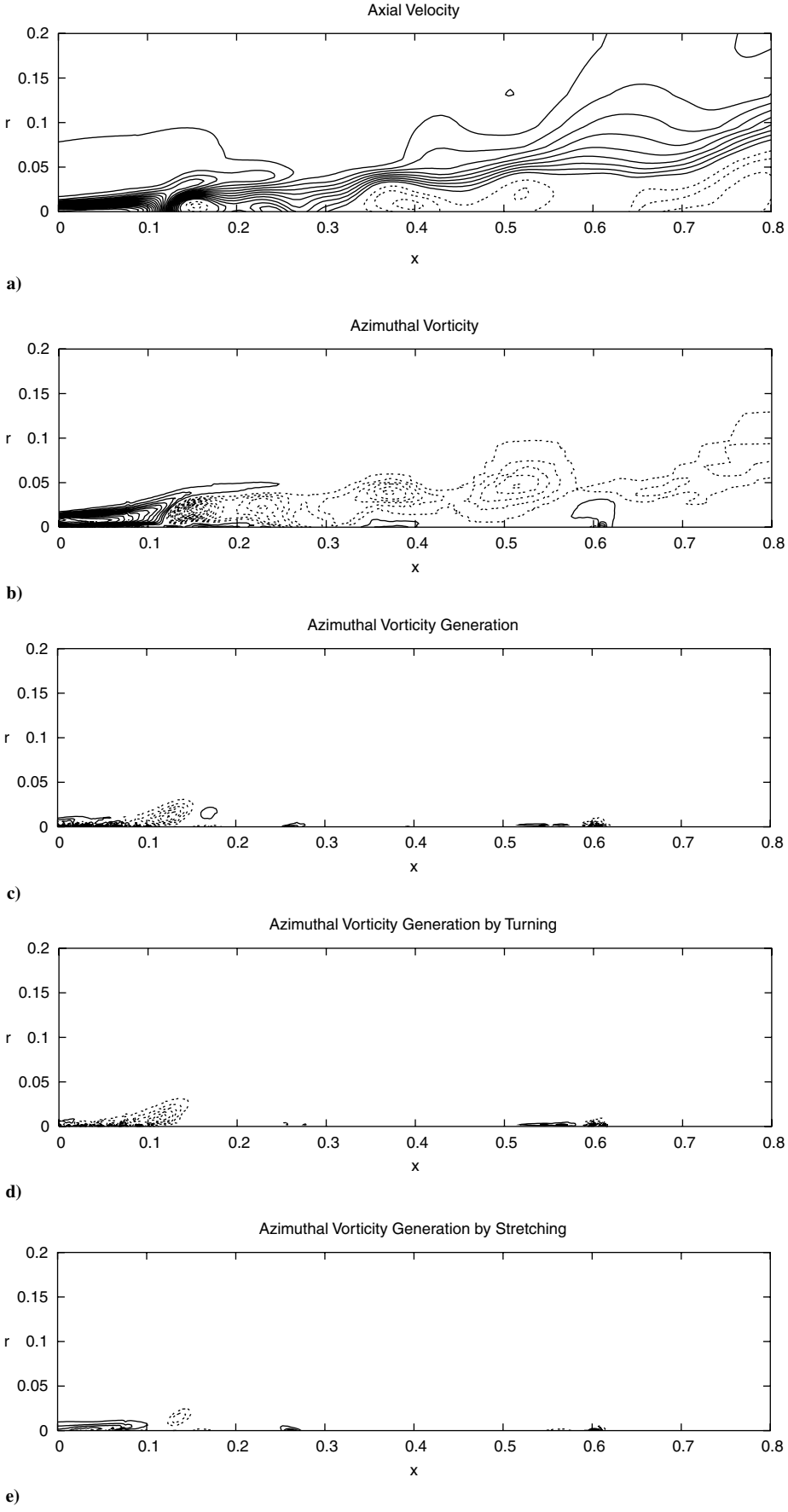

Fig. 14 Delta wing vortex ω_ϕ dynamics for AOA = 40 deg: a) axial velocity, b) ω_ϕ, c) total ω_ϕ generation ($D\omega_\phi/Dt$), d) ω_ϕ generation by turning ($\omega_r \partial u_\phi/\partial r + \omega_x \partial u_\phi/\partial x - u_\phi \omega_r/r$), and e) ω_ϕ generation by stretching ($u_r \omega_\phi/r$).

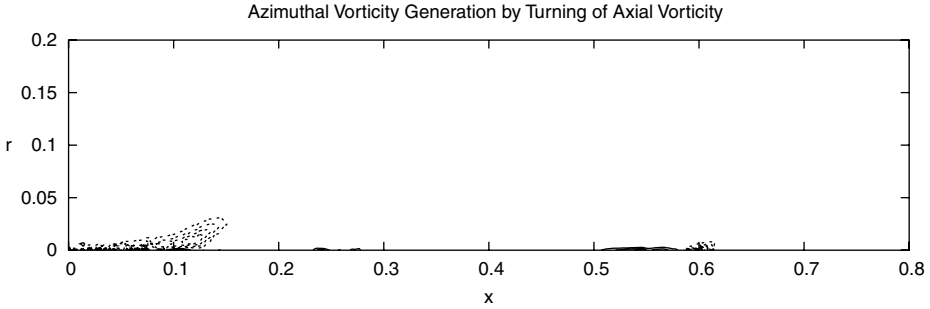

a)

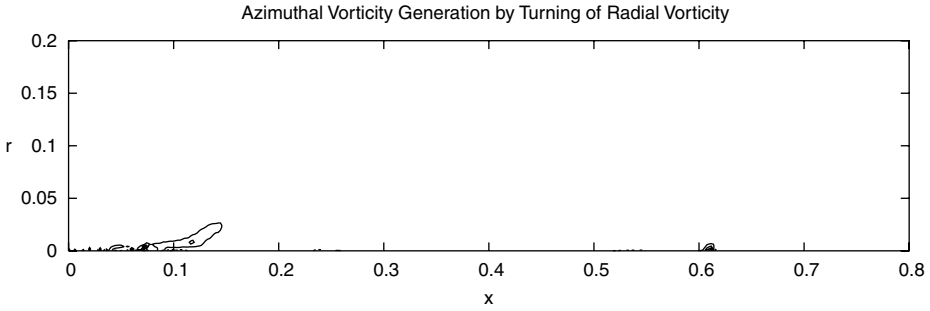

b)

Fig. 15 Delta wing vortex ω_ϕ generation by turning for AOA = 40 deg: a) turning of axial vorticity ($\omega_x \partial u_\phi / \partial x$) and b) turning of radial vorticity ($\omega_r \partial u_\phi / \partial r - u_\phi \omega_r / r$).

from error. Certainly, there are no sizeable structures such as those identified for the higher angles of attack.

VII. Transient Pitching

In the present section, the transient onset of breakdown above a pitching delta wing is examined. Two quantities will be tracked until the onset of breakdown: the azimuthal vorticity and the helix angle.

To validate the present pitching case, we initially adopt a new delta wing geometry to allow comparison with published experimental data. The geometry is identical to that used in the experiment of LeMay et al. [29], shown in Fig. 17. The wing has a thickness of $0.0303c$, and the leading edge has a bevel of 23 deg on the upper and lower surfaces. Again, only half of the wing is modeled, with a symmetry plane at the wing root. Hence, in the current analysis, asymmetry in the solution (such as varying breakdown location on opposing sides of the wing) is not captured. In the experiment [29], smoke was injected into only one vortex; hence, the degree of asymmetry is unknown. The agreement between the computation and experiment will justify the assumption of symmetry here.

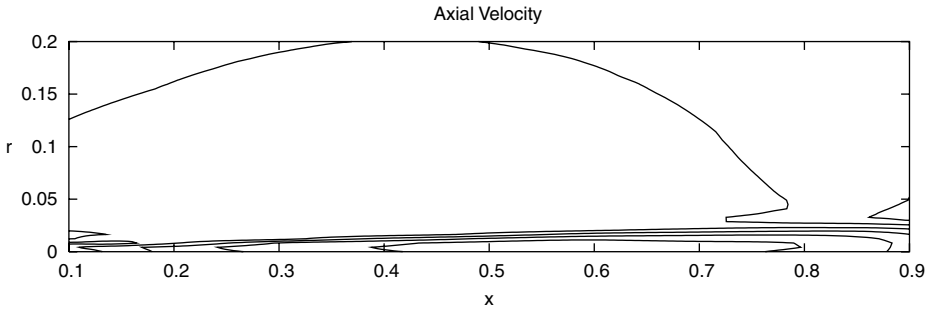

a)

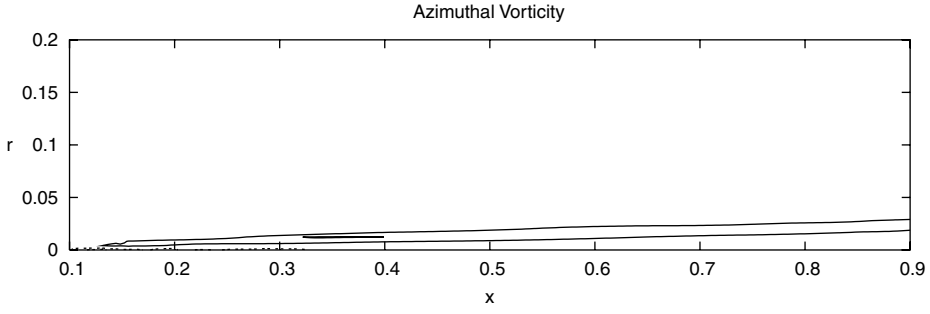

b)

Fig. 16 Delta wing vortex for AOA = 10 deg: a) u_x and b) ω_ϕ.

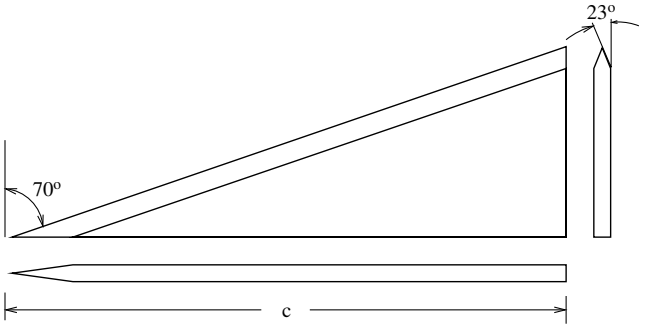

Fig. 17 Delta wing geometry.

Images of the computational mesh are shown in Fig. 18. The mesh is composed of 5.9×10^6 nodes and is single-block, resulting in a singular line at the center of the wing root, on the plane of symmetry. Values on this line are averages of values taken from surrounding cells.

VIII. Validation

In the experiment of LeMay et al. [29], the wing was sinusoidally pitched for two AOA regimes and at various reduced frequencies. For comparison with the current work, we choose the pitching AOA range of 29 to 39 deg and a reduced frequency of $k = 0.30$, which is the highest pitching rate for which experimental results are provided. Vortex breakdown is present over the wing at both extremes of angle of attack; hence, the solution consists of oscillations of breakdown up and down the wing. The intention is to compare the location of breakdown with instantaneous angle of attack in the experiment with that in the computation.

In the experiment, the location of breakdown was defined as the position of initial expansion of the vortex core, determined using smoke visualization. As described by LeMay et al. [29], this point was sometimes difficult to accurately identify, and the measurement was somewhat subjective. An attempt was made to replicate this measurement method for the computational results. A location within the vortex core, well upstream of breakdown, was chosen (the vortex core was identified by determining the local minimum in pressure). This region was seeded with streamlines, as an approximation of the smoke flow visualization used in the experiment. The initial divergence of these streamlines was then used to identify the location of breakdown.

A. Static Case

As an initial condition for the pitching regime, a computational result is obtained for $Re = 2.6 \times 10^5$ and AOA $= 29$ deg. The static location of breakdown in the experiment was $0.86c$. The numerical result gives a location of $0.899c$, a difference of about 5%.

B. Continuous Pitching Case

Continuous sinusoidal pitching is performed in the same manner as in the experiment. Accordingly, the pitching axis is located $0.05c$ below the half-root-chord location. Figure 19 shows the chordwise location of breakdown with instantaneous angle of attack for the experiment and computation (the AOA $= 29$ deg static-wing breakdown locations are also shown, as filled symbols.)

In the experiment, the pitching maneuver was conducted through a minimum of eight cycles and the results were phase-averaged, and in the numerical result, we show an average over two cycles, due to the computational time required for a complete cycle. The initial pitch-up from 29 deg is excluded from the averaging to distance the initial condition from the time-averaged results.

The initial and final locations of breakdown are in agreement to within 6% of c, and the size of the hysteresis loop for the computational model is similar to that in the experiment. Hence, the overall onset and location of breakdown during pitching appears to be reasonably well represented in the calculation.

IX. Pitch-and-Hold Pitching Regime

For the analysis, two pitching regimes are considered: from AOA $= 20$ to 30 deg and from AOA $= 20$ to 40 deg. The final solution at AOA $= 30$ deg contains a breakdown structure at approximately $x = 0.76$, and for AOA $= 40$ deg, breakdown is at approximately $x = 0.46$. However, there is some unsteadiness in the final location of breakdown, as will be seen later.

Each pitching regime consists of three phases (sketched in Fig. 20): 1) ramp up from $\dot{\alpha} = 0$ to a constant pitching rate, 2) constant pitching at rate $\dot{\alpha} = 1.5$ deg/s, and 3) ramp down to $\dot{\alpha} = 0$ and the final AOA.

The pitching rate during the constant pitching phase was chosen to correspond to the reduced frequency of rotation of an 18.5-m-long aircraft at a speed of 247 m/s performing a 20 deg/s pitch-up.

In the preceding study for a static delta wing, the analysis was conducted on a plane that intersected the vortex axis; the analysis was axisymmetric. This was justified on the basis that although the overall flow over the delta wing is three-dimensional, the vortex core is fundamentally axisymmetric. However, because in the present calculation the delta wing moves, the plane on which the analysis is conducted must also move and, in fact, rotate, making it a noninertial frame. The effect of this rotation on the solution has been minimized by maintaining a low pitch-up rate, relative to the freestream velocity.

X. Results: Azimuthal Vorticity

A. AOA = 20 to 30 Degrees

In Figs. 21a–21e, snapshots in time of the azimuthal vorticity in the plane that intersects the vortex core are shown. Only regions in which the azimuthal vorticity is negative are visible (as dark regions). At the base of the plane, a solid line indicates the approximate

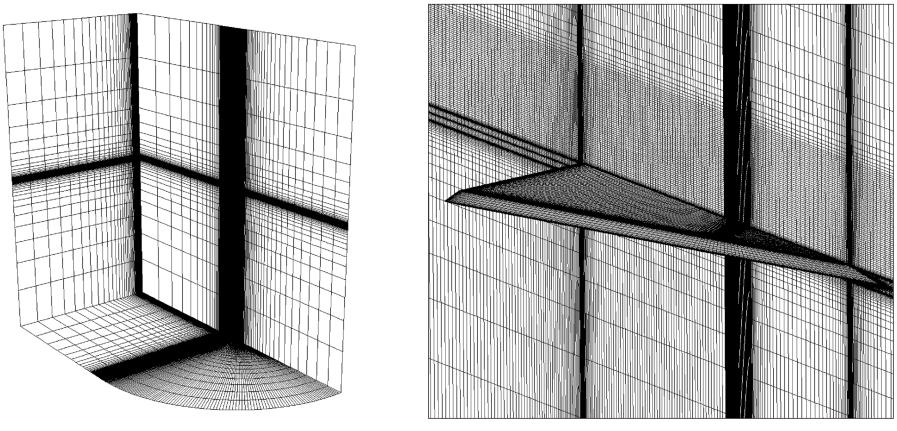

Fig. 18 Computational mesh: complete (left) and close-up (right) views of the wing.

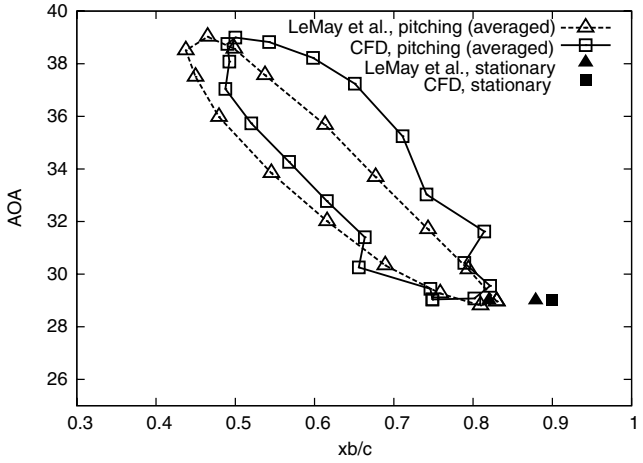

Fig. 19 Breakdown position (x_b/c) vs AOA: computation and experiment (LeMay et al. [29]).

location of the vortex core. A visualization of the wing (almost side-on) is below the plane.

Breakdown will manifest as an axial velocity u_x reversal; regions of negative u_x are visualized as contour lines (only negative levels are plotted). The location of the stagnation point, plus some indication of the shape of the breakdown structure, can be discerned from these regions.

In the initial condition (Fig. 21a), there is some negative azimuthal vorticity present at the edge of the vortex. However, there appears to be no significant negative azimuthal vorticity near the vortex core (the solid line) except near the rear of the wing; just downstream of the trailing edge, a region of negative azimuthal vorticity is present. This region is just upstream of where the vortex core begins to turn upward and merge with the freestream.

At $t = 6$ s [i.e., 6 s after the commencement of pitching (Fig. 21b)], this region of negative azimuthal vorticity has intensified. At $t = 7$ s (Fig. 21c), the first breakdown structure becomes visible downstream of the trailing edge and rapidly grows in size as it moves upstream. By $t = 9$ s (Fig. 21d), breakdown has crossed the trailing edge of the wing, and the pitching has ceased by this time. The region of intensified negative azimuthal vorticity, which appears to sit just outside the zero u isosurface, in fact straddles the surface of the breakdown bubble.

In the last frame (Fig. 21e), breakdown has become established on the core and is still moving upstream. In a later plot (of helix angle), it will be seen to subsequently move a little downstream. A static final location for breakdown is not expected in the computation, because a similar time-varying location was also observed in LeMay et al.'s [29] experiment.

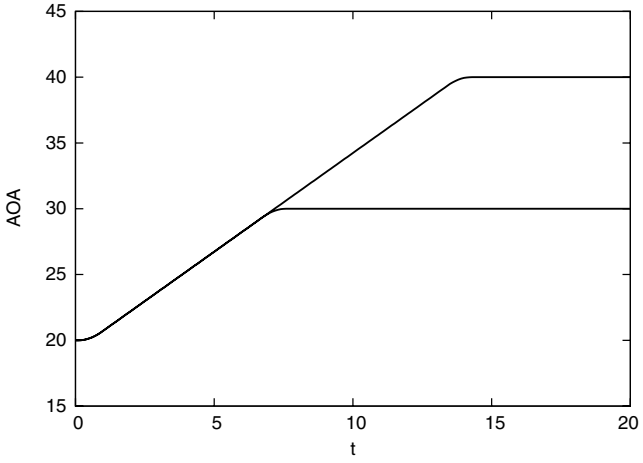

Fig. 20 Ramped pitching regime.

The observation here that breakdown is preceded by the appearance of a region of negative azimuthal vorticity is consistent with conclusions from TDC and pipe studies and also with the delta wing experiment of Lin and Rockwell [30]. The onset of breakdown is also preceded in time by the appearance of negative azimuthal vorticity (Fig. 21b). The appearance and growth of negative ω_ϕ in the region in which breakdown subsequently develops is also consistent with the observations of Darmofal and Murman [7] for an axisymmetric pipe geometry, in which the trapping and amplification of a perturbation to the azimuthal vorticity was linked to the onset of breakdown.

B. AOA = 20 to 40 Degrees

In Figs. 22a–22e, results for the transition for a pitch-up to AOA = 40 deg are shown. The solutions are identical to those for the pitch-up to 30 deg up until that shown in Fig. 21e; hence, that initial phase will not be addressed here. Breakdown for the current case will progress further upstream; hence, the plane is lengthened in the upstream direction.

At $t = 9$ s (Fig. 22a), breakdown has progressed a little further upstream than for the previous pitch-up to 30 deg, as the wing is still pitching. By $t = 11$ s (Fig. 22b), the stagnation region has grown and continues to progress upstream, but its upstream portion maintains a largely axisymmetric form. At $t = 13$ s (Fig. 22c), there is significant loss of symmetry, and by $t = 14$ s (Fig. 22d), a spiral form of breakdown has evolved; the most upstream region of breakdown is no longer stagnant, and hence it is not visualized by the stagnation contours. A region of strongly negative azimuthal vorticity can be seen to precede the onset of the spiral form. The asymmetric spiral structure persists until the final image (Fig. 22e), as do the reversals in azimuthal vorticity just upstream of breakdown.

Hence, similar to the axisymmetric form of breakdown, the appearance of a spiral form of breakdown also coincides with the manifestation of upstream concentrations of negative azimuthal vorticity.

XI. Results: Helix Angle

On the same plane as for the previous vorticity analysis, profiles of instantaneous helix angle are visualized in Fig. 23 for a stationary wing at angles of attack of 20, 30, and 40 deg.

The swirl is relatively high even in the 20 deg AOA case (Fig. 23a), which contains no breakdown. However, the maximum helix angle in this case is $\gamma = 41$ deg, just short of the critical value. For AOA = 30 deg (Fig. 23b), a region of helix angle exceedance ($\gamma \geq 45$ deg) is seen well upstream of breakdown, indicating (according to the criterion) an impending transition in criticality of the vortex core. For AOA = 40 deg, the helix angle also exceeds $\gamma = 45$ deg upstream of breakdown, and the vortex more rapidly (in space) transitions to breakdown. These results indicate that, for a static wing, there is some correspondence between helix angle $\gamma = 45$ deg exceedance and the onset of breakdown. We next track the helix angle for the pitching wing.

A. AOA = 20 to 30 Degrees

We define $\gamma_{\max}$ to be the maximum value of the helix angle in the radial direction at each axial location on the vortex. In Fig. 24, the variation in maximum helix angle $\gamma_{\max}$ with time is shown for the AOA = 20 to 30 deg pitch-up maneuver. The vertical axis is time (in seconds), and the horizontal axis is distance along the vortex core, scaled by c. A black solid line with square markers shows the instantaneous location of the stagnation point associated with breakdown. Only the upper half of the plane is used to calculate $\gamma_{\max}$, as in all cases, the initial helix angle criterion exceedance was observed in the upper half.

In the following analysis, we are only concerned with the region upstream of breakdown. Downstream of the stagnation point (i.e., to the right of the stagnation point in the figure), the helix angle undergoes large fluctuations associated with the highly disturbed flow.

For the transition to AOA = 30 deg, the helix angle first exceeds 45 deg at $t = 2$ s, well before the appearance of breakdown.

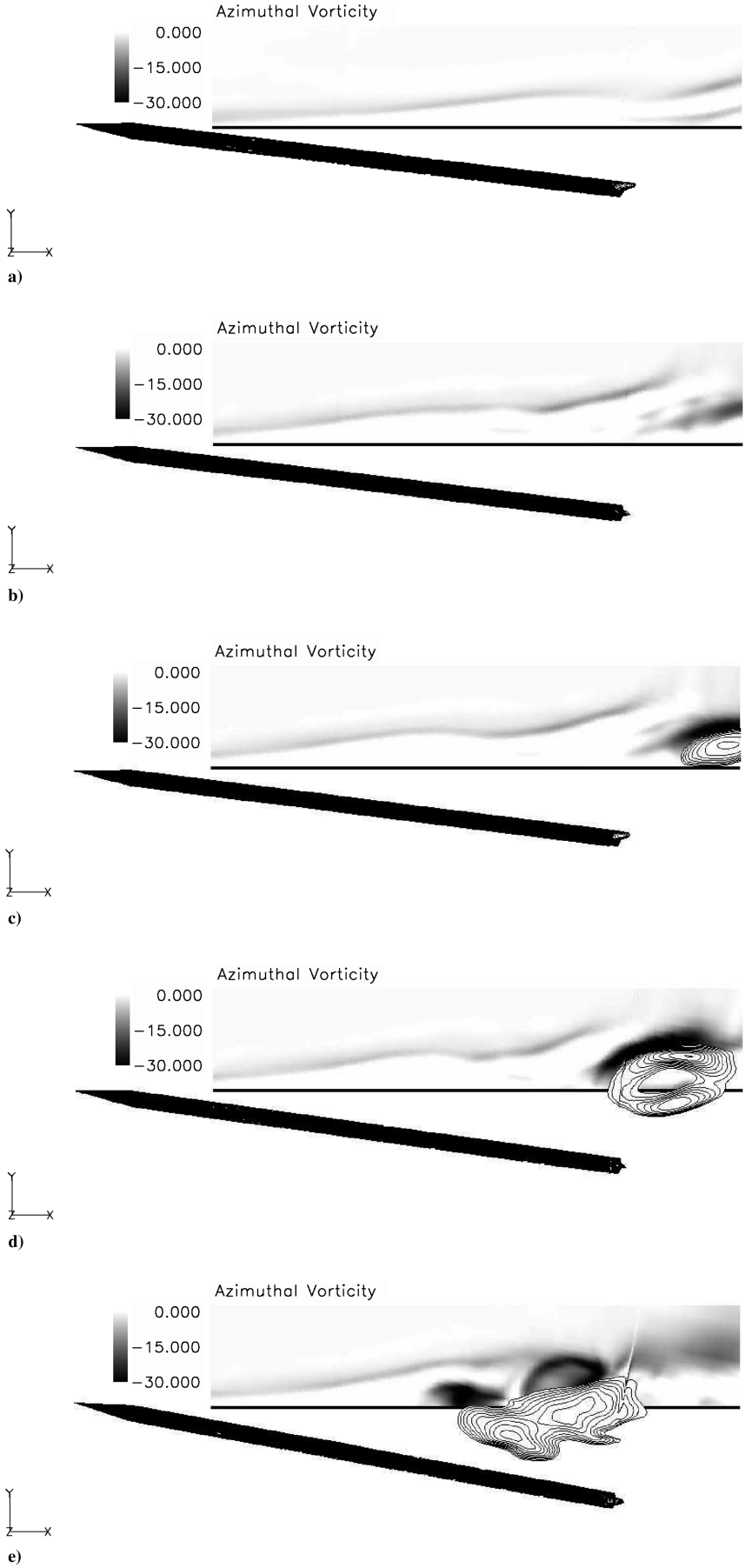

Fig. 21 Images of the azimuthal vorticity associated with a pitch-up from 20 to 30 deg: a) $t = 0$ s, b) $t = 6$ s, c) $t = 7$ s, d) $t = 9$ s, and e) $t = 17$ s.

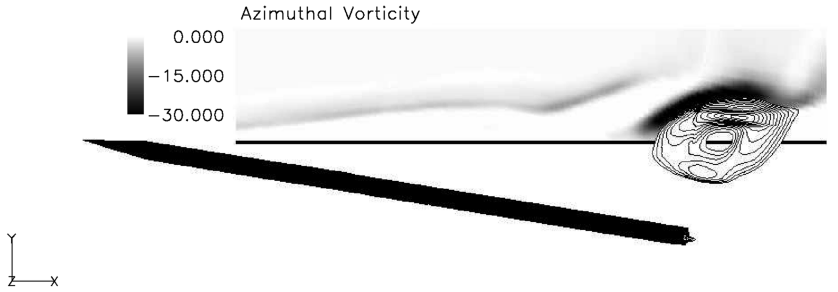

a)

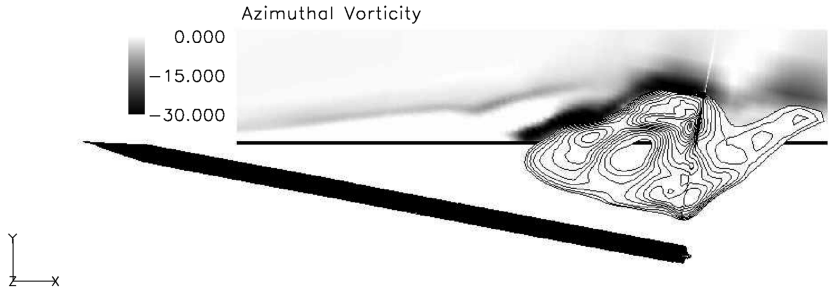

b)

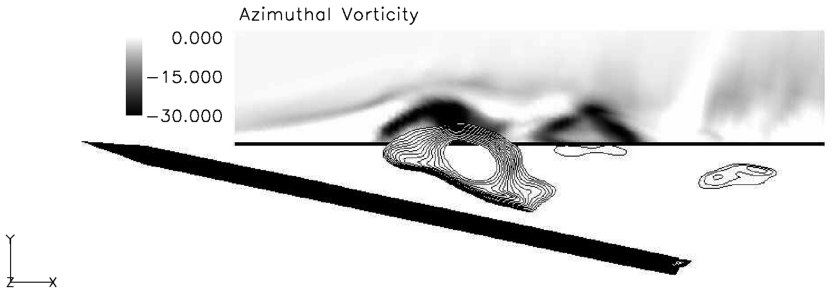

c)

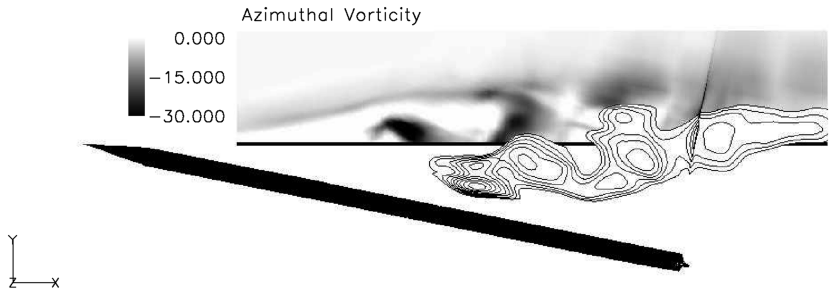

d)

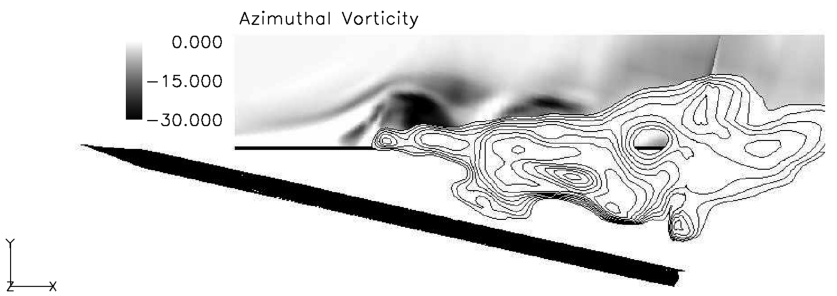

e)

Fig. 22 Images of the azimuthal vorticity associated with a pitch-up from 20 to 40 deg: a) $t = 9$ s, b) $t = 11$ s, c) $t = 13$ s, d) $t = 14$ s, and e) $t = 30$ s.

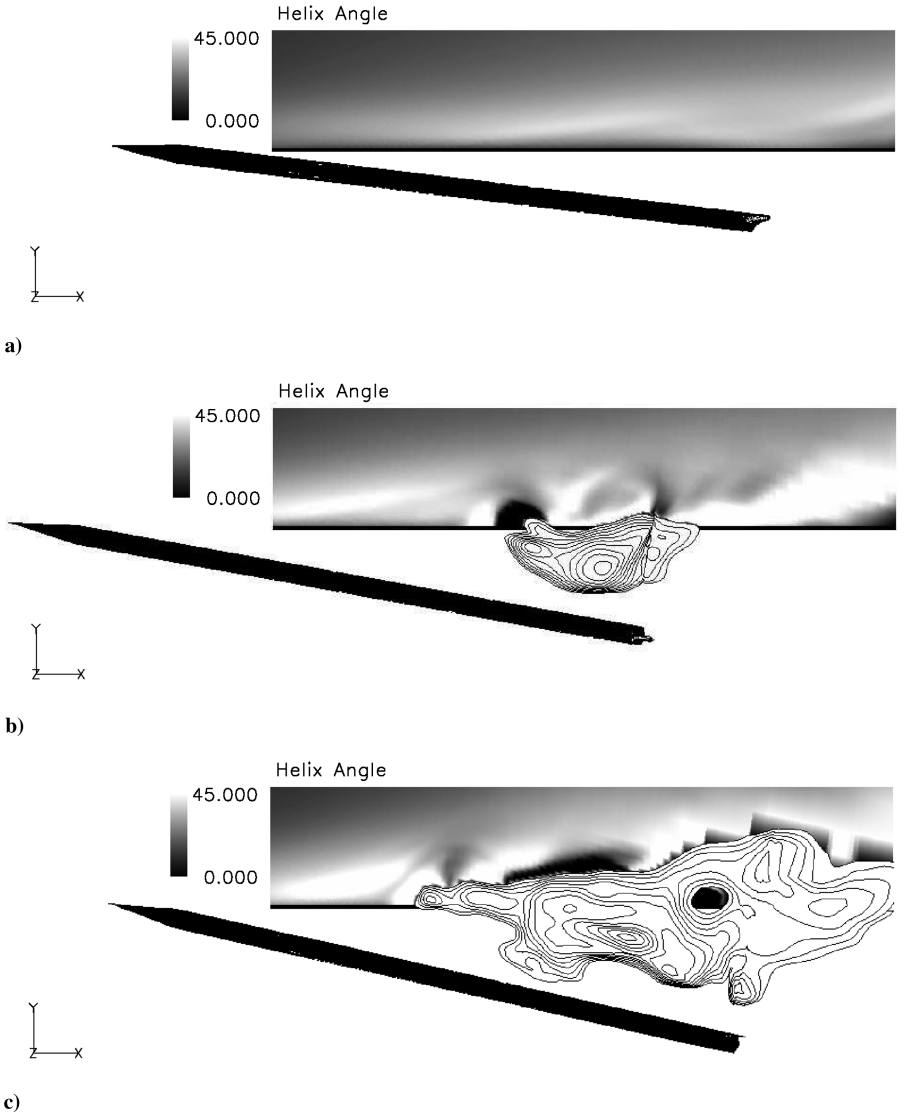

Fig. 23 Instantaneous helix angle for AOA of a) 20 deg, b) 30 deg, and c) 40 deg.

This exceedance occurs at the approximate axial location at which breakdown subsequently develops ($x = 0.925$). A second exceedance appears further upstream of the initial one at about $x = 0.65$ ($t = 4$ s). Breakdown subsequently develops 2 s later and progresses steadily upstream, always preceded by a helix angle exceedance. At $t = 16$ s, breakdown reaches its maximum upstream location. By this time, the helix angle exceedance has become fixed at a location between approximately $x = 0.05$ and 0.25, although breakdown subsequently starts to move downstream.

B. AOA = 20 to 40 Degrees

The helix angle evolution for the pitch-up to 40 deg is shown in Fig. 25. A helix angle $\gamma \geq 45$ deg exceedance is seen from time

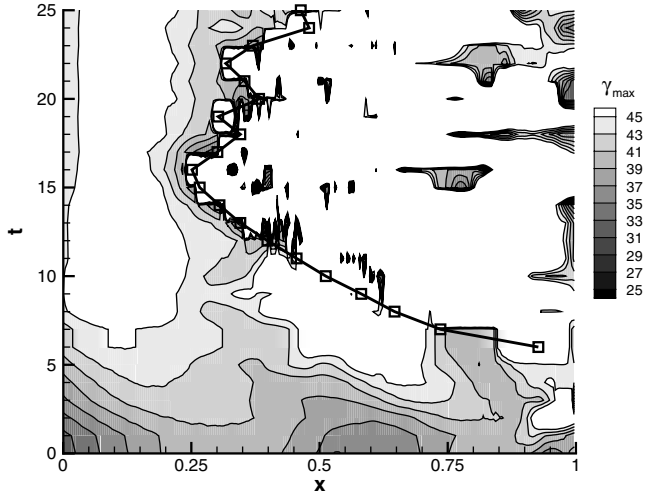

Fig. 24 AOA = 20 to 30 deg pitch-up; helix angle variation with time.

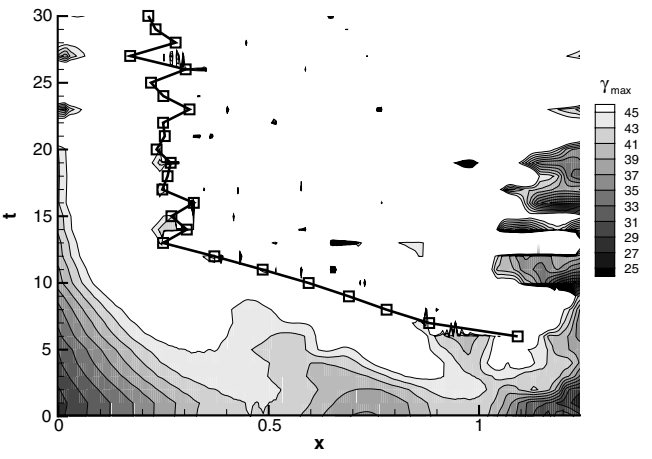

Fig. 25 AOA = 20 to 40 deg pitch-up; helix angle variation with time.

$t = 3$ s; compared with the previous plot, there is a small delay, despite the initial identical nature of the flows. This is due to a slight relocation of the analysis plane for the current case. Similarly to the pitch-up to 30 deg, the helix angle exceedance appears at multiple locations along the vortex core, always in advance of breakdown, which more rapidly migrates upstream in the present case. The initial rapid upstream progression of breakdown slows by $t = 13$ s, after which time the axial location of breakdown oscillates and moves a little upstream, but is always just downstream of the helix angle exceedance. Hence, for the asymmetric and approximately axisymmetric forms of breakdown seen in these transitions, the onset of breakdown appears to coincide with an upstream exceedance of the $\gamma = 45$ deg criterion, both in terms of the time of breakdown's appearance and its location.

XII. Conclusions

The results presented here suggest that the vorticity dynamics associated with vortex breakdown above a high-sweep delta wing are consistent with previous observations for simpler, more confined, geometries. It has been observed that the onset of breakdown is preceded in time and in space by the appearance of azimuthal vorticity ω_ϕ of negative sign. This is consistent with the theory that maintains that the appearance of negative ω_ϕ is a necessary condition for breakdown. The mechanism for the production of this negative ω_ϕ in the vortex core above a delta wing, for moderate Reynolds number, is also in agreement with that observed for a pipe flow at much lower Reynolds number. That is, turning of axial vorticity into the azimuthal direction appears to be the main contributor to the onset of vortex breakdown. Turning of radial vorticity opposes the onset of breakdown. For the current analysis, this mechanism applies for both the axisymmetric bubble and asymmetric spiral forms of breakdown. Compared with the observations for the pipe, stretching does not appear to play as large a part in breakdown onset.

In addition, it has been observed that for the transitions above a delta wing, the onset of breakdown corresponds to an upstream exceedance of the helix angle $\gamma = 45$ deg criterion. Because the $\gamma = 45$ deg criterion indicates a change in the criticality of the vortex core, this observation supports the interpretation of vortex breakdown as a marker of the transition from an upstream supercritical vortex core to a downstream subcritical flow.

Acknowledgment

The authors acknowledge the support of the 21st Century Center of Excellence Program "Frontiers of Computational Science."

References

[1] Maxworthy, T., "Laboratory Modelling of Atmospheric Vortices: A Critical Review," *Topics in Atmospheric and Oceanographic Science: Intense Atmospheric Vortices*, Springer–Verlag, Berlin, 1982, pp. 229–246.

[2] Peckham, D. H., and Atkinson, S. A., "Preliminary Results of Low Speed Wind Tunnel Tests on a Gothic Wing of Aspect Ratio 1.0," *Aeronautical Research Council*, CP 508, London, 1957.

[3] Leibovich, S., "Vortex Stability and Breakdown: Survey and Extension," *AIAA Journal*, Vol. 22, No. 9, 1984, pp. 1192–1206. doi:10.2514/3.8761

[4] Delery, J., "Aspects of Vortex Breakdown," *Progress in Aerospace Sciences*, Vol. 30, No. 1, 1994, pp. 1–59. doi:10.1016/0376-0421(94)90002-7

[5] Althaus, W., Brücker, C., and Weimer, M., "Breakdown of Slender Vortices," *Fluid Vortices*, Kluwer Academic, Boston, 1995, pp. 373–426.

[6] Escudier, M., "Vortex Breakdown: Observations and Explanations," *Progress in Aerospace Sciences*, Vol. 25, No. 2, 1988, pp. 189–229. doi:10.1016/0376-0421(88)90007-3

[7] Darmofal, D., and Murman, E., "On the Trapped Wave Nature of Axisymmetric Vortex Breakdown," AIAA Paper 94-2318, 1994.

[8] Randall, J., and Leibovich, S., "The Critical State: A Trapped Wave Model of Vortex Breakdown," *Journal of Fluid Mechanics*, Vol. 58, No. 3, 1973, pp. 495–515. doi:10.1017/S0022112073002296

[9] Rusak, Z., Wang, S., and Whiting, C., "The Evolution of a Perturbed Vortex in a Pipe to Axisymmetric Vortex Breakdown," *Journal of Fluid Mechanics*, Vol. 366, 1998, pp. 211–237. doi:10.1017/S0022112098001396

[10] Goldshtik, M., and Hussain, F., "Analysis of Inviscid Vortex Breakdown in a Semi-Infinite Pipe," *Fluid Dynamics Research*, Vol. 23, No. 4, 1998, pp. 189–234. doi:10.1016/S0169-5983(98)00016-1

[11] Jones, M., "A Study of the Mechanism for Vortex Breakdown and Some Measures for its Control," Ph.D. Thesis, Monash Univ., Melbourne, Australia, Aug. 2002.

[12] Beran, P., and Culick, F., "The Role of Non-Uniqueness in the Development of Vortex Breakdown in Tubes," *Journal of Fluid Mechanics*, Vol. 242, 1992, pp. 491–527. doi:10.1017/S0022112092002477

[13] Beran, P. S., "The Time-Asymptotic Behavior of Vortex Breakdown in Tubes," *Computers and Fluids*, Vol. 23, No. 7, 1994, pp. 913–937. doi:10.1016/0045-7930(94)90061-2

[14] Lopez, J., "On the Bifurcation Structure of Axisymmetric Vortex Breakdown in a Constricted Pipe," *Physics of Fluids*, Vol. 6, No. 11, Nov. 1994, pp. 3683–3693.

[15] Mitchell, A., and Delery, J., "Research into Vortex Breakdown Control," *Progress in Aerospace Sciences*, Vol. 37, No. 4, 2001, pp. 385–418. doi:10.1016/S0376-0421(01)00010-0

[16] Rusak, Z., and Lamb, D., "Prediction of Vortex Breakdown in Leading-Edge Vortices Above Slender Delta Wings," *Journal of Aircraft*, Vol. 36, No. 4, July–Aug. 1999, pp. 659–667.

[17] Lopez, J., "Axisymmetric Vortex Breakdown Part 1: Confined Swirling Flow," *Journal of Fluid Mechanics*, Vol. 221, 1990, pp. 533–552. doi:10.1017/S0022112090003664

[18] Brown, G. L., and Lopez, J. M., "Axisymmetric Vortex Breakdown Part 2: Physical Mechanisms," *Journal of Fluid Mechanics*, Vol. 221, 1990, pp. 553–576. doi:10.1017/S0022112090003676

[19] Rusak, Z., "Axisymmetric Swirling Flow Around a Vortex Breakdown Point," *Journal of Fluid Mechanics*, Vol. 323, 1996, pp. 79–105. doi:10.1017/S0022112096000857

[20] Wang, S., and Rusak, Z., "The Dynamics of a Swirling Flow in a Pipe and Transition to Axisymmetric Vortex Breakdown," *Journal of Fluid Mechanics*, Vol. 340, 1997, pp. 177–223. doi:10.1017/S0022112097005272

[21] Rusak, Z., Whiting, C. H., and Wang, S., "Axisymmetric Breakdown of a q-Vortex in a Pipe," *AIAA Journal*, Vol. 36, No. 10, Oct. 1998, pp. 1848–1853. doi:10.2514/2.277

[22] Darmofal, D., "A Study of the Mechanisms of Axisymmetric Vortex Breakdown," Ph.D. Thesis, Massachusetts Inst. of Technology, Cambridge, MA, Nov. 1995.

[23] Darmofal, D. L., "The Role of Vorticity Dynamics in Vortex Breakdown," AIAA Paper 93-3036, 1993.

[24] Benjamin, T. B., "Theory of the Vortex Breakdown Phenomenon," *Journal of Fluid Mechanics*, Vol. 14, No. 4, 1962, pp. 593–629. doi:10.1017/S0022112062001482

[25] Spall, R., Gatski, T., and Grosch, C., "A Criterion for Vortex Breakdown," *Physics of Fluids*, Vol. 30, No. 11, 1987, pp. 3434–3440.

[26] Kwak, D., Chang, J. L. C., Shanks, S. P., and Chakravarthy, S. R., "A Three-Dimensional Incompressible Navier-Stokes Flow Solver Using Primitive Variables," *AIAA Journal*, Vol. 24, No. 3, March 1986, pp. 390–396. doi:10.2514/3.9279

[27] Özgören, M., Sahin, B., and Rockwell, D., "Vortex Structure on a Delta Wing at High Angle of Attack," *AIAA Journal*, Vol. 40, No. 2, Feb. 2002, pp. 285–292. doi:10.2514/2.1644

[28] Hall, M., "Vortex Breakdown," *Annual Review of Fluid Mechanics*, Vol. 4, 1972, pp. 195–218. doi:10.1146/annurev.fl.04.010172.001211

[29] LeMay, S., Batill, S., and Nelson, R., "Vortex Dynamics on a Pitching Delta Wing," *Journal of Aircraft*, Vol. 27, No. 2, 1990, pp. 131–138. doi:10.2514/3.45908

[30] Lin, J.-C., and Rockwell, D., "Transient Structure of Vortex Breakdown on a Delta Wing," *AIAA Journal*, Vol. 33, No. 1, 1995, pp. 6–12. doi:10.2514/3.12325

P. Beran
Associate Editor